

Spitzer observations of the Hyades: Circumstellar debris disks at 625 Myr of age

Lucas Cieza^{1,2,3}, William D. Cochran¹, and Jean-Charles Augereau⁴

ABSTRACT

We use the *Spitzer* Space Telescope to search for infrared excess at 24, 70, and 160 μm due to debris disks around a sample of 45 FGK-type members of the Hyades cluster. We supplement our observations with archival 24 and 70 μm *Spitzer* data of an additional 22 FGK-type and 11 A-type Hyades members in order to provide robust statistics on the incidence of debris disks at 625 Myr of age, an era corresponding to the late heavy bombardment in the Solar System. We find that none of the 67 FGK-type stars in our sample show evidence for a debris disk, while 2 out of the 11 A-type stars do so. This difference in debris disk detection rate is likely to be due to a sensitivity bias in favor of early-type stars. The fractional disk luminosity, L_{DUST}/L_* , of the disks around the two A-type stars is $\sim 4 \times 10^{-5}$, a level that is below the sensitivity of our observations toward the FGK-type stars. However, our sensitivity limits for FGK-type stars are able to exclude, at the $2\text{-}\sigma$ level, frequencies higher than 12% and 5% of disks with $L_{DUST}/L_* > 1 \times 10^{-4}$ and $L_{DUST}/L_* > 5 \times 10^{-4}$, respectively. We also use our sensitivity limits and debris disk models to constrain the maximum mass of dust, as a function of distance from the stars, that could remain undetected around our targets.

Subject headings: open clusters and associations: individual (Hyades) — circumstellar matter

¹Astronomy Department and McDonald Observatory, University of Texas, Austin, TX 78712

²Now at the Institute for Astronomy, University of Hawaii at Manoa, Honolulu, HI 96822

³*Spitzer* Fellow

⁴Laboratoire d'Astrophysique de Grenoble, CNRS, Université Joseph-Fourier, UMR 5571, Grenoble, France

1. Introduction

Soon after IRAS discovered cold circumstellar disks around main-sequence (MS) stars (Aumann et al. 1984), it was realized that these disks could not be made of primordial material. Followup CO observations (e.g. Yamashita et al. 1993) showed that molecular gas was highly depleted around these disks. Since, in the absence of gas, the survival time of dust due to dissipation processes such as radiation/wind pressure and the Poynting-Robertson effect is much shorter than the ages of MS stars, these systems are believed to be debris disks where dust is continuously replenished by collisions between planetesimals, the building blocks of planets. Because of their probable connection with the formation of planetary systems, debris disks rapidly became the subject of many studies. However, IRAS was only sensitive enough to study bright nearby objects and most of the pre-*Spitzer* statistics come from surveys performed by IRAS’s successor, the ISO satellite. Habing et al. (2001) studied 84 nearby ($d < 25$ pc) A,F,G, and K stars for which ISO was sensitive to photospheric fluxes and detected $60\ \mu\text{m}$ excess in $\sim 50\%$ of the stars younger than 400 Myr and in 10% of the stars older than 400 Myr. They suggest that this sudden decrease in the fraction of stars with disks around 400 Myr is related to the lifetime of planetesimals that replenish the dust. Spangler et al. (2001) observed ~ 150 pre-main sequence stars and young main sequence stars and detected $60\ \mu\text{m}$ excess in $\sim 25\%$ of the objects. Their observations do not confirm a sudden decrease in the disk fraction around 400 Myr but rather suggest a power law relationship (index ~ -2) between the age of the star and the fractional dust luminosity, L_{DUST}/L_* . They argue that such a power law naturally arises in collisionally replenished debris disks. The discrepancies in the results from these ISO surveys can probably be traced back to the different target selection criteria and observing strategies and to small number statistics. However, since conclusions from Habing et al. (2001) and Spangler et al. (2001) were not totally consistent, ISO was unable to provide a clear picture for the evolution of debris disks.

Fortunately, *Spitzer*’s unprecedented sensitivity has recently allowed many studies of large samples of pre-MS and MS stars in the mid- and far-IR. These studies are rapidly providing important clues on the evolution of debris disks. Rieke et al. (2005) studied over 250 A-type stars and concluded that, even though the incidence of $24\ \mu\text{m}$ excess clearly decreases with increasing stellar age, a very large dispersion on the magnitude of the IR-excesses is seen at every age. Su et al. (2006) finds that A-type stars show a similar qualitative behavior at $70\ \mu\text{m}$. However, at this wavelength, the IR excess declines more slowly with time than at $24\ \mu\text{m}$. The decay timescale is estimated to be ~ 150 Myr for the $24\ \mu\text{m}$ excess and ~ 850 Myr for the $70\ \mu\text{m}$ excess. Trilling et al. (2007) studied field FGK-type stars and found that $\sim 4\%$ and $\sim 16\%$ of them show detectable IR excesses at 24 and $70\ \mu\text{m}$, respectively. These disk frequencies are roughly a factor of two lower than those

found for A-type stars at the same wavelengths. They also find that solar-type stars have an almost constant disk frequency beyond 1 Gyr and hence conclude that their debris disk decay timescale is significantly larger than for A-type star. Gautier et al. (2007) studied a sample of nearby M-type stars but detected no significant far-IR excesses. However, given the sensitivity of their survey, they conclude that the average MIPS excesses, measured in photospheric flux units, of the M-type stars are at least a factor of four lower than those of solar-type stars

The *Spitzer* study of the Hyades presented in this paper is intended to provide additional clues by giving robust statistics on the frequency of debris disks at 625 Myr of age for a homogeneous sample of MS stars. At 46 pc, the Hyades is the nearest star cluster to the Sun, and represent a sample of stars formed at the same epoch with the same heavy element abundance ($[\text{Fe}/\text{H}] = 0.13 \pm 0.01$) (Paulson et al. 2003).

The 625 Myr age of the Hyades places them at an extremely interesting era in the evolution of planetary systems. This age corresponds almost exactly to the era of the late heavy bombardment (LHB) in our Solar System about 3.9 Gyrs ago (Tera et al. 1973). The cratering record of the Moon, Mars, and Mercury all indicate that the inner planets experienced intense bombardment by large bodies at that time. There is still intense debate as to whether the LHB represented merely the end of an exponential decrease in the impact rate from the formation of the terrestrial planets (Wetherill 1975, 1977; Neukum & Ivanov 1994), or was instead a short intense spike in the bombardment rate when the Solar System was about 600 Myr old (Ryder 1990; Cohen 2002). In either case, the LHB of our Solar System clearly indicates that at an age of ~ 600 My there was still a major debris disk present that was undergoing a rapid evolution. Large, asteroid-size bodies had been built up during the early planet building era, but not all of these bodies had been incorporated into the planets. At the time of the LHB, these bodies were undergoing an era of significant collisions with the inner planets, and presumably with each other as well. These collisions would have generated large amounts of smaller particles, ranging all of the way down to dust particles. If most planetary systems go through a LHB-type event at a similar age, it is quite reasonable to assume that other stellar systems might have also similar remnant debris disks at ~ 600 Myr of age. However, it has been recently argued that events such that of the LHB can be triggered by sudden dynamical interactions between planets after a long quiescent period of time (Gomes et al. 2005). In that case, the incidence of debris disks on Hyades members is not expected to be significantly different from that of stars that are somewhat older (or younger) than them.

Here, we analyze deep MIPS 24 and 70 μm observations for a sample of 78 Hyades stars, enough to provide robust statistics on the status of debris disks at 625 Myr of age. In Section

2, we describe the sample of Hyades stars, our observations, and the data reduction procedures. In Section 3, we establish our disk identification criteria and present our detection statistics. In Section 4, we compare our detection statistics to recent *Spitzer* results, use our sensitivity limits and debris disk models to constrain the maximum mass of dust that could remain undetected around our targets, and discuss the implications of our results for debris disk evolution models and the late heavy bombardment in the Solar System.

2. Observations

2.1. *Spitzer* Sample and Observations

The majority of the 78 targets discussed in this paper were observed at 3.6, 4.5, 5.8 and 8.0 μm with the Infrared Array Camera (IRAC) and at 24, 70, and 160 μm with the Multi-band Imaging Photometer for *Spitzer* (MIPS) as part of our General Observer (GO) program 3371. This program contains 45 FGK-type Hyades members from the high-precision radial velocity (RV) survey discussed by Cochran et al. (2002) and Paulson et al. (2004). We have also included MIPS 24 and 70 μm observations of Hyades members from the FEPS *Spitzer* Legacy Project (PID=148, 21 FGK-type stars), and two Guaranteed Time Observation (GTO) programs (PID=40, 11 A-type stars and PID = 71, 1 K0 star). Even though the MIPS photometry for some of the targets has already been discussed in the context of their respective programs (Su et al. 2006; Meyer et al. 2006), we have retrieved the MIPS data from the *Spitzer* archive and processed them ourselves for consistency. The Astronomical Observation Requests (AORs) keys, Program IDs, spectral types from the literature, and near-IR photometry (from 2MASS) for our entire sample of Hyades stars are listed in Table 1.

Given the extreme near-IR brightness of the sample, the IRAC observations of our GO program were acquired in the subarray mode (e.g., 0.02 sec \times 64 frames). The IRAC data were requested to try to better constrain the stellar photospheres of our targets; however, they did not fulfill their intended purpose and were not utilized in our study (see Section 3.1). All the MIPS observations discussed in this paper were obtained using the MIPS pointed imaging mode. At 24 μm , 1 or 2 cycles of 3-sec frames were enough to detect the stellar photospheres of the entire sample with high signal to noise ratio ($S/N > 40$). At 70 μm , the observations were designed for the 1- σ *detector* sensitivities to match the predicted stellar photospheres of the targets. Thus, in the absence of background noise, an IR excess 4 times larger than the photospheric flux would be detected at a 5- σ level. However, at the distance of the Hyades, the 70 μm photospheric emission of most FGK-type stars falls below the extragalactic confusion level (see Section 3.2) and the observations become background limited beyond 24 μm for most of the sample.

2.2. Data Reduction

We processed the IRAC data (available only for the GO program 3371) and MIPS $24\ \mu\text{m}$ data using the mosaicing and source extraction software *c2dphot*, which was developed as part of the the *Spitzer* Legacy Project “From Molecular Cores to Planet Forming Disks” Evans et al. (2006). This program is based on the mosaicking program MOPEX (MOsaicker and Point source EXtractor), developed by the *Spitzer* Science Center (SSC) and on the source extractor program DoPHOT (Schechter et al. 1993). The IRAC and MIPS $24\ \mu\text{m}$ measurements for our entire sample are listed in Tables 2 and 3, respectively.

For the $70\ \mu\text{m}$ and $160\ \mu\text{m}$ data, we used MOPEX to create mosaiced images. We started from the SSC pipeline version S14.4 of the median-filtered BCDs (basic calibrated data), which are optimized for point-source photometry. For each source, we created two versions of the $70\ \mu\text{m}$ mosaic, one resampled to $8''$ pixels (close to the original size of the pixels in the detector) and the other resampled to $4''$ pixels. We used the former to obtain the aperture photometry and the latter to visually inspect the images for background contamination (See section 3.2). The $160\ \mu\text{m}$ data were resampled to mosaics with $16''$ pixels.

For the $70\ \mu\text{m}$ data, we use an aperture of $16''$ in radius and a sky annulus with an inner and an outer radius of $48''$ and $80''$, respectively. From high S/N $70\ \mu\text{m}$ point source observations we derive a multiplicative aperture correction, AC , of 1.8. This AC is in good agreement with the 1.74 value suggested by the *Spitzer* Science Center for observations with the same aperture size and similar sky annulus¹. Thus, we calculate the observed flux, F_{70} , as $F_{70} = FA_{70} \times AC$, where FA_{70} is the flux within the aperture. We estimate the $1\text{-}\sigma$ photometric uncertainty as $\sigma = AC \times RMS_{SKY} \times n^{1/2}$, where RMS_{SKY} is the flux RMS of the pixels in the sky annulus, and n is the number of pixels in our aperture. The $70\ \mu\text{m}$ measurements for our entire sample are listed in Table 3. For the $160\ \mu\text{m}$ data, we used an aperture with a radius of $32''$ and a sky annulus with an inner and an outer radius of $48''$ and $80''$, respectively. The fluxes and uncertainty were calculated in the same way as for the $70\ \mu\text{m}$ data, but adopting an aperture correction of 2.0, appropriate for the size of the aperture and sky annulus used⁴. The $160\ \mu\text{m}$ measurements for the entire sample of FGK-type stars from program ID=3371 are also listed in Table 3 (the $160\ \mu\text{m}$ data are not available for the Hyades stars from the other programs).

¹See <http://ss.spitzer.caltech.edu/mips/apercorr>.

3. Results

3.1. MIPS 24 μm results

At 24 μm , all of our targets are detected with very high signal to noise ratios (S/N \sim 50-300). In order to establish whether or not our targets show IR-excess at a given wavelength, we first need to estimate the expected photospheric fluxes at that wavelength. We do so by normalizing NextGen Models (Hauschildt et al. 1999), corresponding to published spectral types of our Hyades stars, to the near-IR data from 2MASS listed in Table 1. We decided not to include the IRAC data in the normalization of the stellar photospheres for two reasons. First, the IRAC data are only available for the stars from program 3371, and second because we found that including IRAC fluxes does not provide a better photospheric constraint than using the 2MASS data alone. This is probably because, even for bright sources with formal errors $<1\%$, there is a random error floor to the best uncertainty possible with our IRAC and MIPS 24 μm observing techniques and data reduction process of \sim 0.05 mag (Evans et al. 2006). The IRAC photometry for all the targets in our GO program 3371 is presented for completeness only (see Table 2). The expected 24 μm photospheric fluxes for our entire sample, obtained as described above, are listed in Table 3.

The magnitude of the smallest 24 μm excess emission that we can identify depends on both the uncertainty of our photometry and on our ability to predict the photospheric flux. In Figure 1, we plot the distribution of observed 24 μm fluxes relative to predicted photospheric fluxes. After excluding a single outlier, this distribution can be characterized as a Gaussian distribution with a mean of 0.99 and a $1\text{-}\sigma$ dispersion of 0.06. The mean of the distribution is consistent with the absolute *Spitzer* calibration uncertainty at 24 μm . The dispersion of the distribution is identical to that found by Bryden et al. (2006) for FGK-type field stars, smaller than that obtained by Beichman et al. (2007) for FGK, and M stars, and only slightly larger than the uncertainty floor of 0.05 mag expected for 24 μm photometry obtained with *c2dphot* (Evans et al. 2006). However, we note that our $1\text{-}\sigma$ dispersion in the distribution of measured to predicted flux ratios is significantly larger than the \sim 0.03 mag value achieved by Su et al. (2006) for A-type stars and by Thrilling et al. (2007) for FGK-type stars. Based on the analysis of Figure 1, we conclude that only one of the Hyades stars in our sample shows a significant ($> 3\text{-}\sigma$) 24 μm excess. This object is HD28355, an A-type star that was already identified by Su et al. (2006) as having a debris disk. According to the values listed in Table 3, we find that the 24 μm flux of HD28355 is 1.24 times the expected photospheric level, in good agreement with the 1.27 value found by Su et al. (2006).

3.2. MIPS 70 μm results

By extrapolating the *predicted* 24 μm photospheric fluxes, listed in Table 3, we estimated the fluxes of the stellar photospheres that are expected at 70 μm . These predicted 70 μm photospheric fluxes are also listed in Table 3. Unlike at 24 μm , the expected photospheric flux at 70 μm of all our solar-type Hyades stars is at or below the noise of the observations. This noise is dominated by the sky pixel to pixel variations due to extragalactic source confusion and cirrus contamination. Bryden et al. (2006) present a detailed analysis of the sources of noise in deep 70 μm observations. They analyze the noise of images constructed by combining an increasing number of cycles (each cycle consisting of ten 10-sec frames). They show that beyond 4 cycles (a total exposure time of 400 sec), the total noise becomes dominated by the extragalactic background noise. The low spatial resolution of *Spitzer*, combined with the high instrumental sensitivity of MIPS, implies a high incidence of extragalactic sources per beam. This extragalactic source confusion sets a firm limit ($1-\sigma \sim 2$ mJy) to the sensitivity that can be achieved with MIPS at 70 μm . This limit *can not* be reduced with longer integration times. Any contamination from galactic cirrus decreases the sensitivity that can be achieved at any given field. Most of the 70 μm observations discussed in this paper amount to at least 500 sec (and up to 1200 sec in many cases) and hence can be characterized as “background limited”. Since the background noise is highly non-Gaussian, a simple $3-\sigma$ threshold is inappropriate to prevent spurious detections. Thus, the first step in our analysis is to establish a different detection criterion. In Figure 2, we plot the signal to noise ratio as a function of the measured 70 μm flux. We find that a similar number of negative and positive fluctuations exist at the $5-\sigma$ level; therefore, we consider objects with S/N ratios < 5 to be non-detections. We find that only two objects, HD28266 and HD28355, are unambiguously detected. In order to establish that the 70 μm emission is in fact associated with the Hyades targets, we inspect their mosaics, shown in Figure 3, and verify that the emission is centered on the targets. HD28266 and HD28355 are both A-type stars, which have been already identified by Su et al. (2006) as having a debris disk. As mentioned in Section 3.1, HD28355 also shows significant 24 μm excess.

Three objects, HD27962, HD29488, and HD33524, have S/N just above 5. We consider these objects to be possible detections that need further consideration. We inspect their high resolution (4" pixel) mosaics (Figures 4 and 5) to establish the spatial distribution of the 70 μm emission. In the three cases we find that even though there seems to be a source near the aperture, there is a significant offset ($\sim 10-15''$) between the center of the 70 μm emission and the location of the Hyades target. Therefore, we conclude that the 70 μm emission within these apertures are likely to be due to background contamination.

We note that one of these objects, HD33524, has been identified by Su et al. (2006) as

having a weak $70\ \mu\text{m}$ excess. For this object, they report a $70\ \mu\text{m}$ flux of 21.46 ± 2.17 mJy as opposed to our 18.5 ± 3.25 mJy (i.e., the fluxes agree very well within the uncertainties). A similar situation occurs for HD28527. Su et al. (2006) report a $70\ \mu\text{m}$ flux of 37.36 ± 5.94 mJy, which also is in relative agreement with our 25.1 ± 5.08 measurement (within $\sim 2\sigma$). However, since the $70\ \mu\text{m}$ emission does not seem to be centered at the target (Figure 5), we do not consider this detection to be real either. An independent reanalysis and inspection of the $70\ \mu\text{m}$ data of HD 33254 and HD 28527 confirms that the $70\ \mu\text{m}$ fluxes within the apertures are no likely to be associated with the Hyades stars (Su 2008, private communications). Our conservative detection criterion is also supported by the presence of negative background fluctuations at the $5\text{-}7\sigma$ level at the location of some of the targets, such as HD28430 shown in Figure 6.

We conclude that none of the 67 FGK-type Hyades stars in our sample are detected at $70\ \mu\text{m}$, while 2 of the 11 A-type stars are. The measured $70\ \mu\text{m}$ fluxes for these two objects, HD28266 and HD28355, are 13.9 and 11.5 times the values predicted for their respective photospheres (see Table 3). We attribute these excesses, as Su et al. (2006) did, to the presence of debris disks around both of these sources.

3.3. MIPS $160\ \mu\text{m}$ results

At $160\ \mu\text{m}$, the expected photospheric levels are significantly below the noise of the observations (which are only available for the 45 FGK-type stars from the program ID=3371). In order to establish the detection of any of our targets, we follow the same approach as for the $70\ \mu\text{m}$ data. In Figure 7, we plot the the signal to noise ratio as a function of the measured $160\ \mu\text{m}$ flux. As for the $70\ \mu\text{m}$ observations, we find that a similar number of negative and positive fluctuations exist at the $5\text{-}\sigma$ level; therefore, we considered all the $160\ \mu\text{m}$ measurements to be non-detections.

4. Discussion

4.1. Comparison to Recent Spitzer Results

Recent *Spitzer* surveys have provided robust statistics on the debris disk frequencies around nearby stars against which our results can be compared. In order to make more meaningful comparisons, we divide the sample into FGK-type stars (67 objects) and A-type stars (11 objects). There are two motivations for doing so. First, most of the previous studies are restricted to either one of these groups. Second, given the strong luminosity dependence

on spectral type, the $70\ \mu\text{m}$ observations are sensitive to much smaller $70\ \mu\text{m}$ excesses (in units of photospheric fluxes) and L_{DUST}/L_* values for A-type stars than for FGK-type stars.

4.1.1. FGK-type vs A-type stars

To estimate the sensitivity difference between the $70\ \mu\text{m}$ observations of A-type stars and FGK-type stars, we calculate the ratio of 5 times the flux uncertainties to the estimated photospheric values (from Table 3). A cumulative histogram of this ratio is shown in Figure 8 for FGK and A-type stars. For A-type stars, the $70\ \mu\text{m}$ observations can detect fluxes that are $\sim 1\text{-}2\times$ those of the expected photospheres. However, for most of the FGK-type stars, the $70\ \mu\text{m}$ observations are only sensitive enough to detect fluxes that are $\sim 15\times$ the expected photospheric values. As discussed in Section 3.2, this sensitivity limitation is mostly due to the fact that the stellar photospheres of solar-type stars, at the distance of the Hyades, fall below the $70\ \mu\text{m}$ extragalactic confusion limit for MIPS ($1\text{-}\sigma \sim 2\ \text{mJy}$, Bryden et al. 2006).

The difference in $70\ \mu\text{m}$ sensitivity is even larger when it is calculated in terms of minimum detectable disk luminosity, L_{DUST}/L_* . Following Bryden et al. (2006), we calculate minimum disk luminosity as a function of $70\ \mu\text{m}$ excess flux by setting the emission peak at $70\ \mu\text{m}$ ($T_{DUST} = 52.5\text{K}$), according to:

$$\frac{L_{DUST}}{L_*}(\text{minimum}) = 10^{-5} \left(\frac{5600\text{K}}{T_*} \right)^3 \frac{F_{DUST,70}}{F_{*,70}} \quad (1)$$

where $F_{DUST,70}$ is the flux of the dust and $F_{*,70}$ is the flux of the stars, both at $70\ \mu\text{m}$. By setting $F_{DUST,70} = 5\sigma_{70} - F_{*,70}$, we calculate the minimum L_{DUST}/L_* values that are detectable for A-type and FGK-type stars. The results are shown in Figure 9, which demonstrates that the $70\ \mu\text{m}$ observations of A-type stars are sensitive enough to detect disk with L_{DUST}/L_* values in the $10^{-6}\text{-}10^{-5}$ range. However for most of the FGK-type stars, the $70\ \mu\text{m}$ observations are only sensitive enough to detect disks with $L_{DUST}/L_{STAR} \gtrsim 1\text{-}2 \times 10^{-4}$. We also use equation 1 to estimate L_{DUST}/L_* values of 3.4×10^{-5} and 4.7×10^{-5} for the debris disks around HD28226 and HD28355, respectively. Since there are only 2 FGK-type objects for which the $70\ \mu\text{m}$ observations are sensitive enough to detect disks fainter than $L_{DUST}/L_* \sim 4.0 \times 10^{-5}$, we conclude that the difference in the detection rate of debris disks around A-type stars and FGK-type stars is the result of a sensitivity bias rather than a real effect.

4.1.2. Comparison to FGK-type field stars

Bryden et al. (2006) present 24 and 70 μm observations for 69 FGK nearby (distance $\sim 10\text{-}30$ pc) field stars with a median age of ~ 4 Gyrs. They find 24 μm excess around only one of their targets. This is consistent with the 24 μm excess rate of 0% we find for our 67 FGK-type stars. At 70 μm , they identify 7 debris disks. This excess rate ($\sim 10\%$), if taken at face value, seems inconsistent with our results. However, given the smaller distances to the stars involved, their survey was more sensitive than ours to faint disks. Since the stellar photospheres of their targets are above the 70 μm confusion limit of MIPS, they were able to detect the stellar photosphere of most of them and identify very faint disks ($L_{DUST}/L_* \geq 10^{-5}$). They also find that the disk frequency increases from $2\% \pm 2\%$ for disks with $L_{DUST}/L_* \geq 10^{-4}$ to $12\% \pm 5\%$ for disks with $L_{DUST}/L_* \geq 10^{-5}$. Recent results by Trilling et al. (2008) confirm that the frequency of debris disks with $L_{DUST}/L_* \geq 10^{-4}$ around solar type stars is $\sim 2\%$.

Figure 9 shows that there are only 22 objects for which our 70 μm observations are sensitive enough to detect a debris disk with $L_{DUST}/L_* \geq 10^{-4}$. We use binomial statistics to show that if the incidence of disks brighter than $L_{DUST}/L_* = 10^{-4}$ is in fact 2% as found by Bryden et al. (2006) and Trilling et al. (2007), there was a 26% probability that our survey would find zero disks. Also, given the cumulative distribution of sensitivities shown in Figure 9, we use binomial statistics to calculate the minimum disk frequencies, as a function of L_{DUST}/L_* , that would be *excluded* at the 1- and 2- σ level (i.e., the disk frequencies that would give our survey a 32% and 5% chance to result in zero detections). These disk frequencies are tabulated in Table 4.

Based on the statistics for disks with $L_{DUST}/L_* \geq 10^{-4}$, Table 4 suggests that a debris disk fraction in the Hyades ~ 2.5 and ~ 6 times larger than in the field can be excluded at the 1- σ and 2- σ level, respectively. Thus, we conclude that the debris disk fraction of the FGK-type Hyades stars (age ~ 625 Myr) is consistent with that in the field (age ~ 4 Gyrs), but that $\sim 6\times$ higher values cannot be excluded from the currently available data.

4.2. Comparison to debris disk models

In this section, we use the debris disk model developed by Augereau et al. (1999) to constrain the location and mass of the circumstellar material around HD 28266 and HD 28355, the two A-type stars identified in section 3.2 as having real 70 μm excesses. We also use this model to estimate the maximum encompassed mass of dust, as a function of distance from the stars, that could remain undetected around the A-type and FGK-type stars in our

sample that do not show significant IR excesses.

4.2.1. The debris disks around HD 28266 and HD 28355

We limit the exploration of the parameter space to the disk parameters that affect most the global shape of an SED, namely the minimum grain size a_{\min} , the peak surface density position r_0 and the total dust mass M_{dust} (or, equivalently, the surface density at r_0). We adopted a differential grain size distribution proportional to $a^{-3.5}$ between a_{\min} and a_{\max} , with $a_{\max} = 1300 \mu\text{m}$, a value sufficiently large to not affect the SED fitting in the wavelength range we consider. Following Augereau et al. (1999), the disk surface density $\Sigma(r)$ is parametrized by a two power-law radial profile $\Sigma(r) = \Sigma(r_0)\sqrt{2}(x^{-2\alpha_{\text{in}}} + x^{-2\alpha_{\text{out}}})^{-1/2}$ with $x = r/r_0$, and where $\alpha_{\text{in}} = 10$ and $\alpha_{\text{out}} = -3$ to simulate a disk peaked around r_0 , with a sharp inner edge, and a density profile decreasing smoothly with the distance from the star beyond r_0 . The optical properties of the grains were calculated for astronomical silicates (optical constants from Weingartner & Draine (2001)), and with the Mie theory valid for hard spheres. The grain temperatures were obtained by assuming the dust particles are in thermal equilibrium with the central star. NextGen model atmosphere spectra (Hauschildt et al. 1999) scaled to the observed K-band magnitudes, were used to model the stellar photospheres.

For each of the stars with $70 \mu\text{m}$ excess, HD 28266 and HD 28355, we calculated 15000 SEDs ($0.3 \mu\text{m} \leq \lambda \leq 950 \mu\text{m}$), for 75, logarithmically-spaced values of a_{\min} between $0.05 \mu\text{m}$ and $100 \mu\text{m}$, and for 200 values of r_0 , logarithmically-spaced between 10 AU and 500 AU. For each model, the dust mass was adjusted by a least-squares method, assuming purely photospheric emission in the 2MASS bands and by fitting the measured MIPS $24 \mu\text{m}$ and $70 \mu\text{m}$ flux densities. The results are summarized in Table 5, and the SEDs are displayed in Figure 10. Results in Table 7 are listed for two different regimes of minimal grain sizes, namely, $a_{\min} > 10 \mu\text{m}$ and $a_{\min} < 0.5 \mu\text{m}$ in order to illustrate the strong dependence of r_0 and M_{dust} on the assumed grain size distribution.

Even though neither the position of the peak surface density r_0 , nor the minimum grain size a_{\min} , can be uniquely determined with so few observational constraints, some models can be eliminated. In particular, given the large luminosity of A-type stars, the small or nonexistent excess at $24 \mu\text{m}$ implies that the disks of HD 28226 and HD 28355 are significantly dust-depleted within *at least* ~ 40 AU from the star. However, “inner-holes” larger than 300 AU can not be excluded if very small grains are present (i.e., $a_{\min} < 0.5 \mu\text{m}$). Similarly, even though the best-fit disk models imply dust masses of the order $10^{-2}M_{\oplus}$, disk masses $\sim 0.1M_{\oplus}$ could be accommodated for both stars.

4.2.2. Limits on dust masses as a function of radius

In section 4.1.1, we found that the 70 μm observations of the Hyades were sensitive to significantly lower fractional disk luminosities for A-type stars than for FGK-type stars. However, since the 70 μm observations probe larger radii around A-type stars than around FGK-stars, this implies that the mass of the grains needed to produce a given fractional luminosity, as calculated in section 4.1.1, is *larger* around A-type stars than it is around FGK-type stars (see Gautier et al. 2007 for a discussion of origin of the dependence of dust mass sensitivity on stellar luminosity). Therefore, the degree to which the MIPS observations are sensitive to smaller amounts of dust around A-type stars than around FGK-type stars is not immediately obvious. In order to explore this last point, we estimate the maximum encompassed mass of dust, as a function of distance from the stars, that could remain undetected around the A-type and FGK-type stars in our sample that do not show significant IR excesses.

Following Cieza et al. (2007), we use the optically thin disk models discussed above to constrain the maximum amount of dust that could be present within 300 AU of the A-type and FGK-type stars in our sample. Using the 70 μm 5- σ upper limits (and the 160 μm limits, when available), we calculated 15000 models analogous to those calculated for HD 28266 and HD 28355 for each of the stars in our sample. For each model, we calculated the mass encompassed within a radius r , as a function of this radius. With this approach, we estimate the maximum dust mass in the circumstellar regions of the Hyades stars with no detectable emission in excess to the photospheric emission. The results for A-type and FGK-type stars, for two different minimal grain size regimes ($a_{\text{min}} > 10 \mu\text{m}$ in blue and $a_{\text{min}} < 0.5 \mu\text{m}$ in red), are shown in Figure 11. This figure shows that the absence of IR excess at 24 and 70 μm constrains the total mass of dust within 10 AU of the solar type stars to be $< 10^{-4} M_{\text{Earth}}$. This limit is an order of magnitude lower for A-type stars. The range of encompassed dust masses as a function of radius for the best-fit disk models of HD 28355 corresponding to the case where $a_{\text{min}} > 10 \mu\text{m}$ is shown for comparison (green region). The fact that, for FGK-type stars, the green region lies below the blue region (i.e., the case corresponding to the same grain size distribution), implies that disks similar to that found around HD 28355 would not be detectable by our observations if they were also present around the FGK-type Hyades members. Given the similarities of the inferred disk properties of HD 28355 and HD 28266 (see Table 5), the same conclusion applies for HD 28266. Thus, Figure 11 strengthen our conclusion from section 4.1.1 stating that the difference in detection rate of debris disks around A-type and FGK-type stars is due to a sensitivity bias rather than to a real difference in the incidence or properties of debris disks around stars of different spectral types.

4.3. Debris disk evolution and the Late Heavy Bombardment

4.3.1. Steady State vs. Stochastic Evolution

Rieke et al. (2005) studied a sample of 266 A-type stars with *Spitzer*, ISO, or IRAS 24 μm /25 μm data. They used this very large sample to establish statistically significant trends of IR-excess with age. They find that: (1) at all ages, the population is dominated by stars with little or no IR excess, (2) stars with a wide range of excesses are seen at every age, and (3) both the frequency and the magnitude of the IR excess decreases with time. In particular, they find that the upper envelope of the evolution of the excess ratio with time can be fitted by t_o/t , with $t_o \sim 150$ Myr. Similar trends are seen in the 70 μm excesses of A-type stars (Su et al. 2006), with the difference that the decay time seems to be considerably larger, $t_o \gtrsim 400$ Myr, suggesting inside-out disk clearing.

Based on these results, Rieke et al. (2005) argue that the evolution of debris disks is the convolution of a stochastic and a steady component. They suggest that, at any given age, the debris disks detected are those that have experienced large planetesimal collisions in the recent past. This stochastic evolution is on top of steady decrease in the number of parent bodies in the belts of planetesimals where the dust is produced, which would explain the overall decrease of IR excess with age. However, it has also been argued that a stochastic component in the evolution of debris disk is not necessary to explain the diversity of disk properties observed at a given age. Wyatt et al. (2007b) construct a simple collisional model, where the mass of planetesimals is constant until the largest ones reach collisional equilibrium, at which point mass falls as 1/time. They propose that the large spread in IR properties observed at any given age can be explained in terms of the initial distributions of masses and temperatures of the planetesimal belts producing the dust. They argue that their simple model can account for the 24 and 70 μm statistics presented by Rieke et al. (2005) and Su et al. (2006) using realistic belt parameters, and thus that transient events are not *required* to explained the observations. Given the limited observational constraints available, the models presented by Wyatt et al. (2007b) do not rule out the possibility that stochasticity plays an important role in the evolution of most debris disks. Our results could provide additional constrains to these kinds of models because, unlike the studies by Rieke et al. (2005) and Su et al. (2006), our study provides robust statistics for the debris disks at a single, well defined age.

4.3.2. *Implications for the Late Heavy Bombardment in the Solar System*

The 625 Myr age of the Hyades corresponds almost exactly to the era of the late heavy bombardment (LHB, Tera et al. 1973; Gomes et al. 2005). Thus, *if* the Solar-type (FGK) Hyades stars resemble the Sun at 625 Myr of age, our statistics could provide valuable clues on this important event in the history of the Solar System.

The cause and the duration of the LHB is still a matter of debate. Proposed causes for a intense spike in the impact rate include the formation of Uranus and Neptune (Levison et al. 2001), the presence of a fifth terrestrial planet in a low-eccentricity orbit which became dynamically unstable at an age of about 600 Myr (Chambers & Lissauer 2002), or impacts by bodies left over from planetary accretion (Morbidelli et al. 2001). More recently, Gomes et al. (2005) propose that the LHB was triggered by the sudden migration of the giant planets that occurred after a long quiescent period of time. In their model, soon after the dissipation of the solar nebula, the orbits of Jupiter and Saturn started to slowly diverge due to the interaction with the massive disk of planetesimals that was still present. They argue that ~ 700 Myr later, when Jupiter and Saturn crossed their 1:2 mean motion resonance, their orbits became eccentric and temporally destabilized those of Uranus and Neptune. The reconfiguration of the orbits of the giant planets resulted in the perturbation and massive delivery of planetesimals to the inner Solar System, which according to their models, lasted between 10-150 Myr.

The observational signatures of a LHB-type event as seen from a distance of 46 pc are not known, but it has been suggested that they could be those of a family of rare Solar-type stars characterized by the presence of a bright “hot disk” around an object hundreds of million years old. These objects present excess IR emission, originating in the terrestrial planet regions, with $F_{DUST}/F_* > 10^{-4}$, a level that is > 1000 times larger than steady state evolution models can explain (Wyatt et al. 2007a). There are currently only 5 known objects that fall into this category of “hot transient disks”: BD +20 307 (age ~ 300 Myr, Song et al. 2005), HD72905 (age ~ 400 Myr, Beichman et al. 2006), η Corvi (age ~ 1 Gyr, Wyatt et al. 2005), HD69830 (age ~ 2 Gyr, Beichman et al. 2005), and τ Ceti (age ~ 10 Gyr, Di Folco et al. 2007) which represent $\sim 2\%$ of all the Solar-type stars surveyed. *If* this group of objects corresponds to those that are currently experiencing events similar to the LHB and the Hyades stars resemble the Sun at 625 Myr of age, then the fact that none of the 67 Solar-type stars in our Hyades sample has a “hot transient disk” implies one of two possibilities: (1) the likelihood of an event similar to the LHB is not significantly higher at ~ 625 Myr than it is at any other age, or (2) events like the LHB are very short spikes with a duration much closer to the lower limit of 10 Myr suggested by Gomes et al. (2005) than to their 150 Myr upper limit. If the likelihood of a LHB-type event is approximately constant with time, then

a 2% incidence in the Solar neighborhood (median age ~ 4000 Myr) would imply a total duration of ~ 80 Myr. However, if such an event is more likely to occur around an age of ~ 625 Myr, then our non detections would only be consistent with a much shorter duration. Thus, the implication of our results on the LHB could depend on the age distribution of these “hot transient disks”, which still remains largely unconstrained since only 5 of such examples are currently known. Fortunately, as more *Spitzer* observations are reported, this distribution will become better constrained.

Understanding the debris disk phenomenon has been a high priority of the *Spitzer*'s mission. As a result, the number of debris disk studies has increased dramatically over the last few years. Each of these studies is providing new clues and constraints, from which it will eventually emerge a much clearer picture of the evolution of debris disks and its connection to the history of the Solar System.

We thank the anonymous referee for his/her many comments and suggestions, which have helped to improve the paper significantly. We are deeply grateful to Diane Paulson for helping to stimulate this work and for valuable assistance in preparing the target lists. This work is based on observations and on archival data obtained with the Spitzer Space Telescope, which is operated by the Jet Propulsion Laboratory, California Institute of Technology under a contract with NASA. Support for this work was provided by NASA through an award issued by JPL/Caltech and through the Spitzer Space Telescope Fellowship Program. This publication makes use of the data products from the Two Micron All Sky Survey, which is a joint project of the University of Massachusetts and the Infrared Processing and Analysis Center/California Institute of Technology, funded by the National Aeronautics and Space Administration and the National Science Foundation.

REFERENCES

- Augereau, J. C., Lagrange, A. M., Mouillet, D., Papaloizou, J. C. B., & Grorod, P. A. 1999, *A&A*, 348, 557
- Aumann, H. H., Beichman, C. A., Gillett, F. C., de Jong, T., Houck, J. R., Low, F. J., Neugebauer, G., Walker, R. G., & Wesselius, P. R. 1984, *ApJ*, 278, L23
- Beichman, C. A., Bryden, G., Rieke, G. H., Stansberry, J. A., Trilling, D. E., Stapelfeldt, K. R., Werner, M. W., Engelbracht, C. W., Blaylock, M., Gordon, K. D., Chen, C. H., Su, K. Y. L., & Hines, D. C. 2005, *ApJ*, 622, 1160
- Beichman, C. A., Bryden, G., Stapelfeldt, K. R., Gautier, T. N., Grogan, K., Shao, M., Velusamy, T., Lawler, S. M., Blaylock, M., Rieke, G. H., Lunine, J. I., Fischer, D. A., Marcy, G. W., Greaves, J. S., Wyatt, M. C., Holland, W. S., & Dent, W. R. F. 2006, *ApJ*, 652, 1674
- Beichman, C. A., Fridlund, M., Traub, W. A., Stapelfeldt, K. R., Quirrenbach, A., & Seager, S. 2007, in *Protostars and Planets V*, ed. B. Reipurth, D. Jewitt, & K. Keil, 915–928
- Bryden, G., Beichman, C. A., Trilling, D. E., Rieke, G. H., Holmes, E. K., Lawler, S. M., Stapelfeldt, K. R., Werner, M. W., Gautier, T. N., Blaylock, M., Gordon, K. D., Stansberry, J. A., & Su, K. Y. L. 2006, *ApJ*, 636, 1098
- Cieza, L., et al. 2007, *ApJ*, 667, 308
- Chambers, J. E., & Lissauer, J. J. 2002, in *LPI Conference Abstracts*, 1093
- Cochran, W. D., Hatzes, A. P., & Paulson, D. B. 2002, *AJ*, 124, 565
- Cohen, B. A. 2002, in *LPI Conference Abstracts*, 1984
- Di Folco, E., et al. 2007, *A&A*, 475, 243
- Evans, N. J., et al. 2003, *PASP*, 115, 965
- Evans, N. J., Harvey, P. M., Dunham, M. M., Mundy, L. G., Lai, S., Chapman, N., Huard, T., Brooke, T. Y., & Koerner, D. W. 2006, *Delivery of Data from the c2d Legacy Project: IRAC and MIPS (Pasadena,SSC)*, Pasadena, SSC, <http://ssc.spitzer.caltech.edu/legacy/original.html>
- Gautier, T. N., III, et al. 2007, *ApJ*, 667, 527
- Gomes, R., Levison, H. F., Tsiganis, K., & Morbidelli, A. 2005, *Nature*, 435, 466

- Habing, H. J., Dominik, C., Jourdain de Muizon, M., Laureijs, R. J., Kessler, M. F., Leech, K., Metcalfe, L., Salama, A., Siebenmorgen, R., Trams, N., & Bouchet, P. 2001, *A&A*, 365, 545
- Hauschildt, P. H., Allard, F., & Baron, E. 1999, *ApJ*, 512, 377
- Levison, H. F., Dones, L., Chapman, C. R., Stern, S. A., Duncan, M. J., & Zahnle, K. 2001, *Icarus*, 151, 286
- Meyer, M. R., Hillenbrand, L. A., Backman, D., Beckwith, S., Bouwman, J., Brooke, T., Carpenter, J., Cohen, M., S. Cortes, S., Crockett, N., Gorti, U., Henning, T., Hines, D., Hollenbach, D., Kim, J. S., Lunine, J., R. Malhotra, E. M., Metchev, S., Moro-Martin, A., Morris, P., Najita, J., Padgett, D., Pascucci, I., Rodmann, J., Schlingman, W., Silverstone, M., Soderblom, D., Stauffer, J., Stobie, E., Strom, S., Watson, D., Weidenschilling, S., & S. Wolf, E. Y. 2006, *PASP*, 118, 1690
- Morbidelli, A., Petit, J.-M., Gladman, B., & Chambers, J. 2001, *Meteoritics and Planetary Science*, 36, 371
- Neukum, G., & Ivanov, B. A. 1994, in *Hazards Due to Comets and Asteroids*, 359
- Paulson, D. B., Cochran, W. D., & Hatzes, A. P. 2004, *AJ*, 127, 3579
- Paulson, D. B., Sneden, C., & Cochran, W. D. 2003, *AJ*, 125, 3185
- Rieke, G., Su, K. Y. L., Stansberry, J. A., Trilling, D., Bryden, G., Muzerolle, J., White, B., Gorlova, N., Young, E. T., Beichman, C. A., Stapelfeldt, K. R., & Hines, D. C. 2005, *ApJ*, 620, 1010
- Ryder, G. 1990, *EOS*, 71, 313
- Schechter, P. L., Mateo, M., & Saha, A. 1993, *PASP*, 105, 1342
- Song, I., Zuckerman, B., Weinberger, A. J., & Becklin, E. E. 2005, *Nature*, 436, 363
- Spangler, C., Sargent, A. I., Silverstone, M. D., Becklin, E. E., & Zuckerman, B. 2001, *ApJ*, 555, 932
- Su, K. Y. L., Rieke, G. H., Stansberry, J. A., Bryden, G., Stapelfeldt, K. R., Trilling, D. E., Muzerolle, J., Beichman, C. A., Moro-Martin, A., Hines, D. C., & Werner, M. W. 2006, *ApJ*, 653, 675
- Tera, F., Papanastassiou, D. A., & Wasserburg, G. J. 1973, in *LPI Conf. Abstracts*, 723

- Trilling, D. E., et al. 2007, ArXiv e-prints, 710, arXiv:0710.5498
- Weingartner, J. C., & Draine, B. T. 2001, ApJ, 548, 296
- Wetherill, G. W. 1975, in Lunar and Planetary Science Conference, 1539
- Wetherill, G. W. 1977, in Lunar and Planetary Science Conference, 1
- Wyatt, M. C., Greaves, J. S., Dent, W. R. F., & Coulson, I. M. 2005, ApJ, 620, 492
- Wyatt, M. C., Smith, R., Greaves, J. S., Beichman, C. A., Bryden, G., & Lisse, C. M. 2007a, ApJ, 658, 569
- Wyatt, M. C., Smith, R., Su, K. Y. L., Rieke, G. H., Greaves, J. S., Beichman, C. A., & Bryden, G. 2007b, ApJ, 663, 365
- Yamashita, T., Handa, T., Omodaka, T., Kitamura, Y., Kawazoe, E., Hayashi, S. S., & Kaifu, N. 1993, ApJ, 402, L65

Table 1. Sample of Hyades Stars

Star Name	Ra (J2000.0)	Dec (J2000.0)	MIPS AOR	IRAC AOR	PID	Spectral Type	J (mag)	H (mag)	K _S (mag)
BD+17 455	43.81800	17.89170	10853888	10865152	3371	G7	7.56	7.21	7.18
BD+29 503	44.44480	29.66140	10841856	10854400	3371	K0	7.38	7.00	6.91
HD 18632	45.01220	7.74980	10842112	10854656	3371	K2	6.32	5.95	5.84
HD 20430	49.35990	7.65580	05403904	...	148	F8	6.29	6.05	5.99
BD+07 499	50.12200	8.45440	12289280	12288512	3371	K5	7.54	6.96	6.88
BD+23 465	53.20890	23.69240	10842624	10855168	3371	K1	7.37	7.02	6.91
HIP 17766	57.04970	7.14620	10843648	10856192	3371	K6	8.27	7.62	7.51
BD+23 571	57.76320	23.90360	10843904	...	3371	K7	8.11	7.54	7.39
HD 286363	58.75610	12.48560	10854144	10856704	3371	K4	8.18	7.69	7.57
HD 285252	58.77730	16.99840	10844160	10856960	3371	K2	7.41	7.04	6.91

Note. — The complete version of this table is in the electronic edition of the Journal. The printed edition contains only a sample.

Table 2. IRAC Photometry

Star name	Ra (J2000.0)	Dec (J2000.0)	3.6 μm Flux (mJy)	4.5 μm Flux (mJy)	5.8 μm Flux (mJy)	8.0 μm Flux (mJy)
BD+17 455	43.81795	17.89166	384	251	149	65
BD+29 503	44.44457	29.66151	482	286	166	98
HD 18632	45.01211	7.74987	1390	800	498	300
BD+07 499	50.12181	8.45457	462	279	170	99
BD+23 465	53.20876	23.69213	500	278	157	91
HIP 17766	57.04950	7.14626	302	156	117	59
HD 286363	58.75592	12.48568	250	143	95	54
HD 285252	58.77703	16.99855	454	297	163	93
BD+19 650	60.91259	19.45522	233	135	92	50
HIP 19082	61.35694	19.44221	160	82	64	33

Note. — [1]The complete version of this table is in the electronic edition of the Journal. The printed edition contains only a sample.]

Note. — [2] A 5% error should be adopted for all IRAC fluxes. As discussed in Section 3.1, even though the formal errors in our IRAC measurements are typically $<1\%$, there is a random error floor to the best uncertainty possible with our IRAC observing techniques and data reduction process of $\sim 5\%$]

Table 3. MIPS photometry and photospheric predictions

Star name	Flux24 (mJy)	σ 24 (mJy)	P24 (mJy)	Flux70 (mJy)	σ 70 (mJy)	P70 (mJy)	Flux160 (mJy)	σ 160 (mJy)	P160 (mJy)
BD+17 455	9.72	0.095	10.4	-0.97	3.00	1.22	21.1	12.50	0.23
BD+29 503	12.2	0.093	14.0	-5.07	2.82	1.64	7.8	30.60	0.31
HD 18632	33.8	0.171	33.1	5.96	4.31	3.90	82.9	22.50	0.74
HD 20430	28.1	0.097	29.3	11.10	4.58	3.45
BD+07 499	13.3	0.096	13.8	0.81	2.98	1.62	-39.3	33.00	0.31
BD+23 465	12.4	0.093	13.2	-1.97	2.37	1.55	-20.6	36.90	0.29
HIP 17766	7.89	0.080	7.31	-8.01	2.55	0.85	-11.0	12.60	0.16
BD+23 571	8.23	0.086	9.15	3.07	2.55	1.08	-15.7	17.70	0.20
HD 286363	7.06	0.060	7.06	0.76	1.69	0.83	-23.6	9.89	0.15
HD 285252	12.2	0.092	12.4	-2.04	3.22	1.46	-53.5	25.60	0.27

Note. — The complete version of this table is in the electronic edition of the Journal. The printed edition contains only a sample.

Table 4. Disk Frequency Limits

$L_{DUST}/L_* \geq$	Number of stars above limit	1- σ	2- σ
1×10^{-4}	22	5.0%	12.7 %
2×10^{-4}	47	2.4%	6.2%
5×10^{-4}	64	1.8%	4.6%
1×10^{-3}	67	1.7%	4.4%

Table 5: Optically thin disk properties, for two different regimes of minimal grain sizes a_{\min} .

Star Name	$a_{\min} > 10 \mu\text{m}$		$a_{\min} < 0.5 \mu\text{m}$	
	r_0 (AU)	$M_{\text{dust}} (10^{-3} M_{\oplus})$	r_0 (AU)	$M_{\text{dust}} (10^{-3} M_{\oplus})$
HD 28226	46^{+26}_{-13}	$9.4^{+24}_{-6.9}$	475^{+24}_{-192}	52^{+20}_{-19}
HD 28355	$39^{+11}_{-9.2}$	$10^{+16}_{-7.5}$	383^{+116}_{-150}	57^{+21}_{-23}

24 μm RESULTS

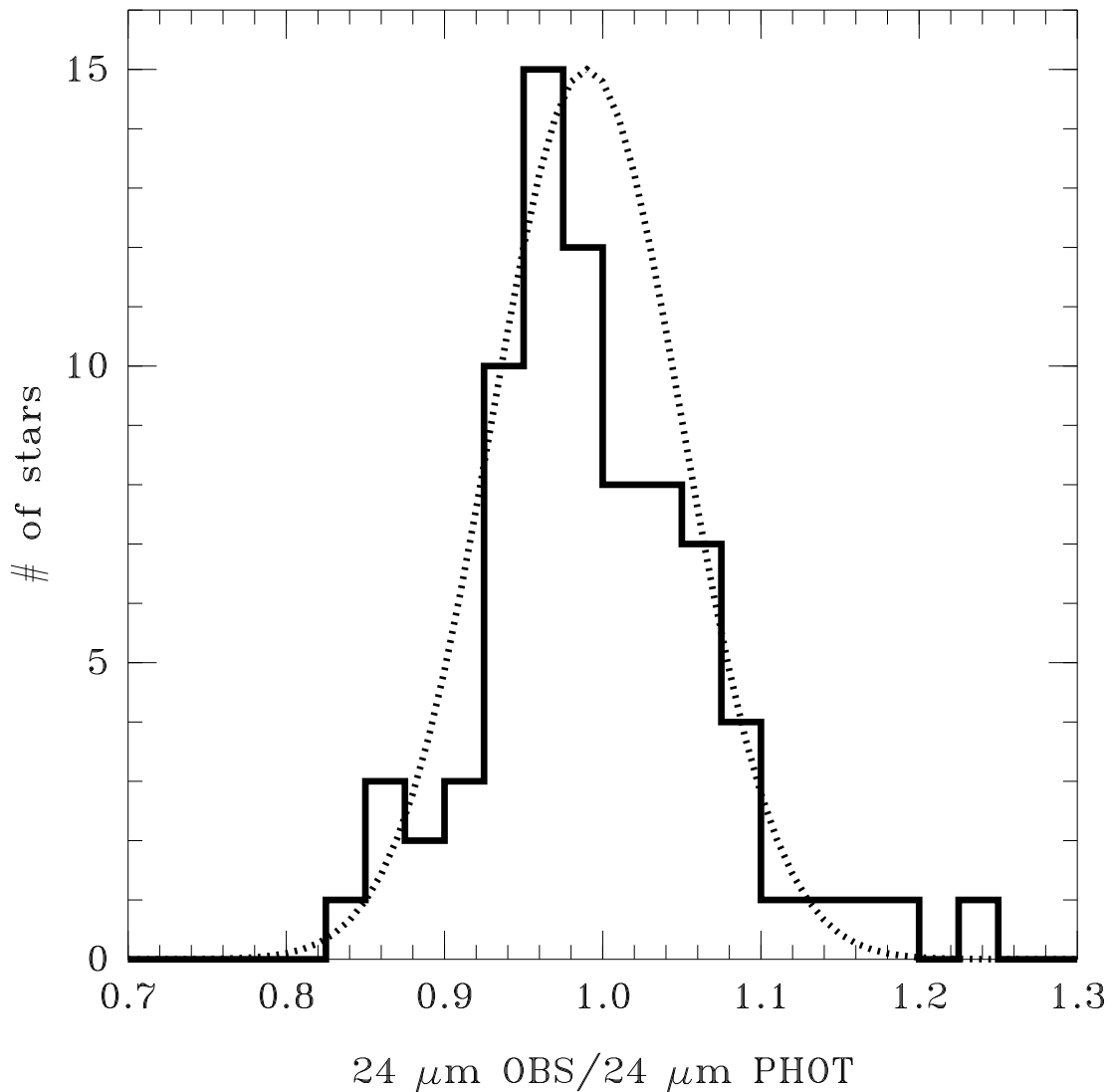


Fig. 1.— Distribution of the observed 24 μm fluxes in units of the expected photospheric fluxes. A Gaussian distribution centered at 0.99 and with a 1- σ dispersion of 0.06 (dotted line) is shown for comparison. Only one object, HD28355, shows a significant ($> 3\text{-}\sigma$) 24 μm excess above the predicted stellar photosphere. HD28355 is an A-type star whose excess was already identified by Su et al. (2006).

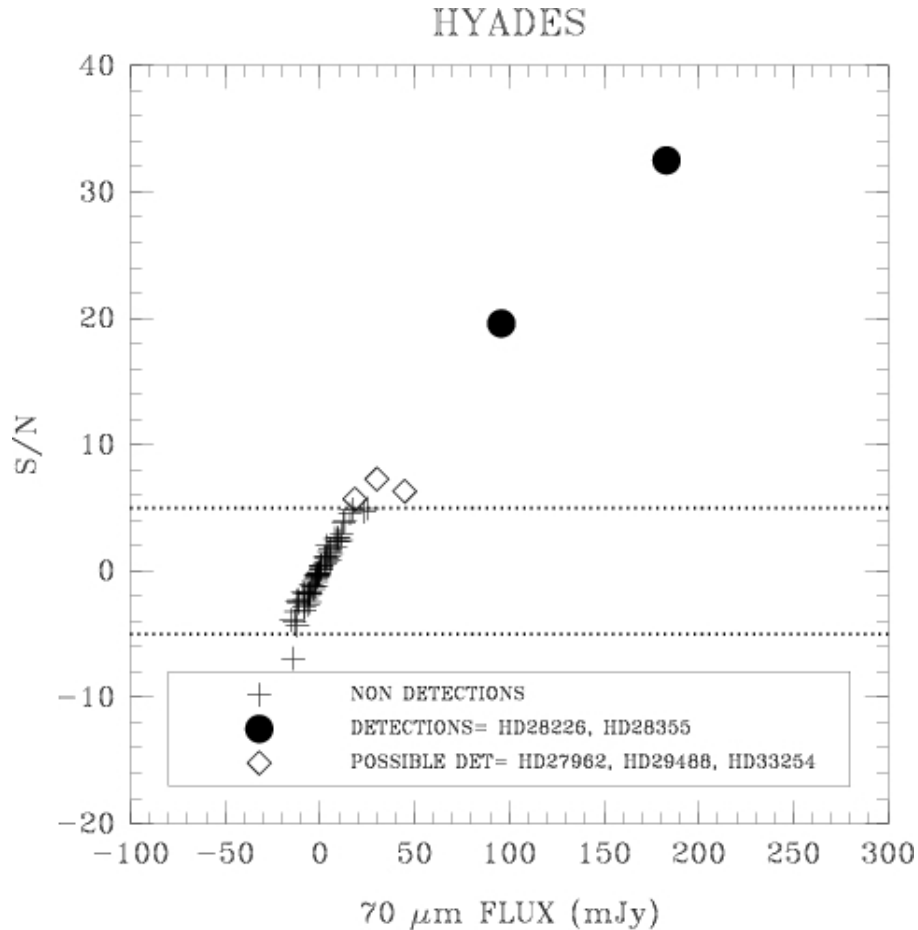


Fig. 2.— The signal to noise ratio versus the measured $70\ \mu\text{m}$ flux for our sample of Hyades stars. Two objects shown as filled circles, HD28226 and HD28355, clearly stand out as robust detections. The horizontal dotted lines delimit the $5 > S/N > -5$ interval. For the deep $70\ \mu\text{m}$ observations considered in this paper, the noise is dominated by the sky background variations. This variations are highly none Gaussian and primarily due to extragalactic source confusion and cirrus contamination. As a result, there is a similar number of objects with $S/N \sim 5$ and with $S/N \sim -5$ and we consider objects $S/N < 5$ to be none detections. Three objects, HD27962, HD29488, and HD33524, have S/N just above 5. We consider these objects to be possible detections that need further consideration.

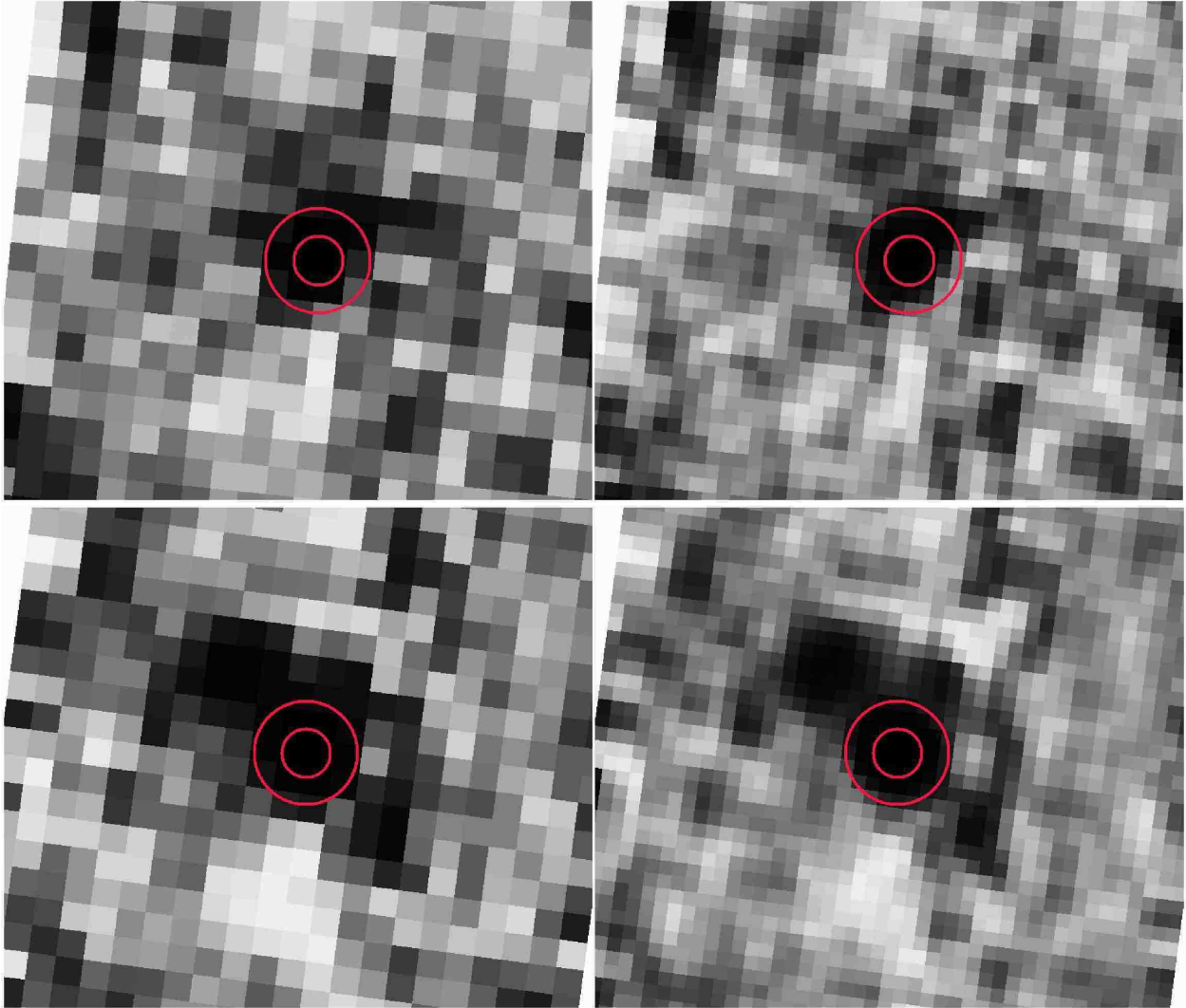


Fig. 3.— The $70\ \mu\text{m}$ *inverted* grayscale mosaics of HD28226 (top) and HD28355 (bottom). North is up and East is to the left in all the images. The images on the left correspond to the mosaics with $8''$ pixels (close to the physical size of the detector). The image on the right correspond to the mosaics resampled to $4''$ pixels (\sim half the physical size). The $70\ \mu\text{m}$ emissions are centered at the positions of the objects (marked by the concentric circles) and are detected with signal to noise ratios ~ 20 -30. Both objects are A-type stars already identified by Su et al. (2006) as having debris disks.

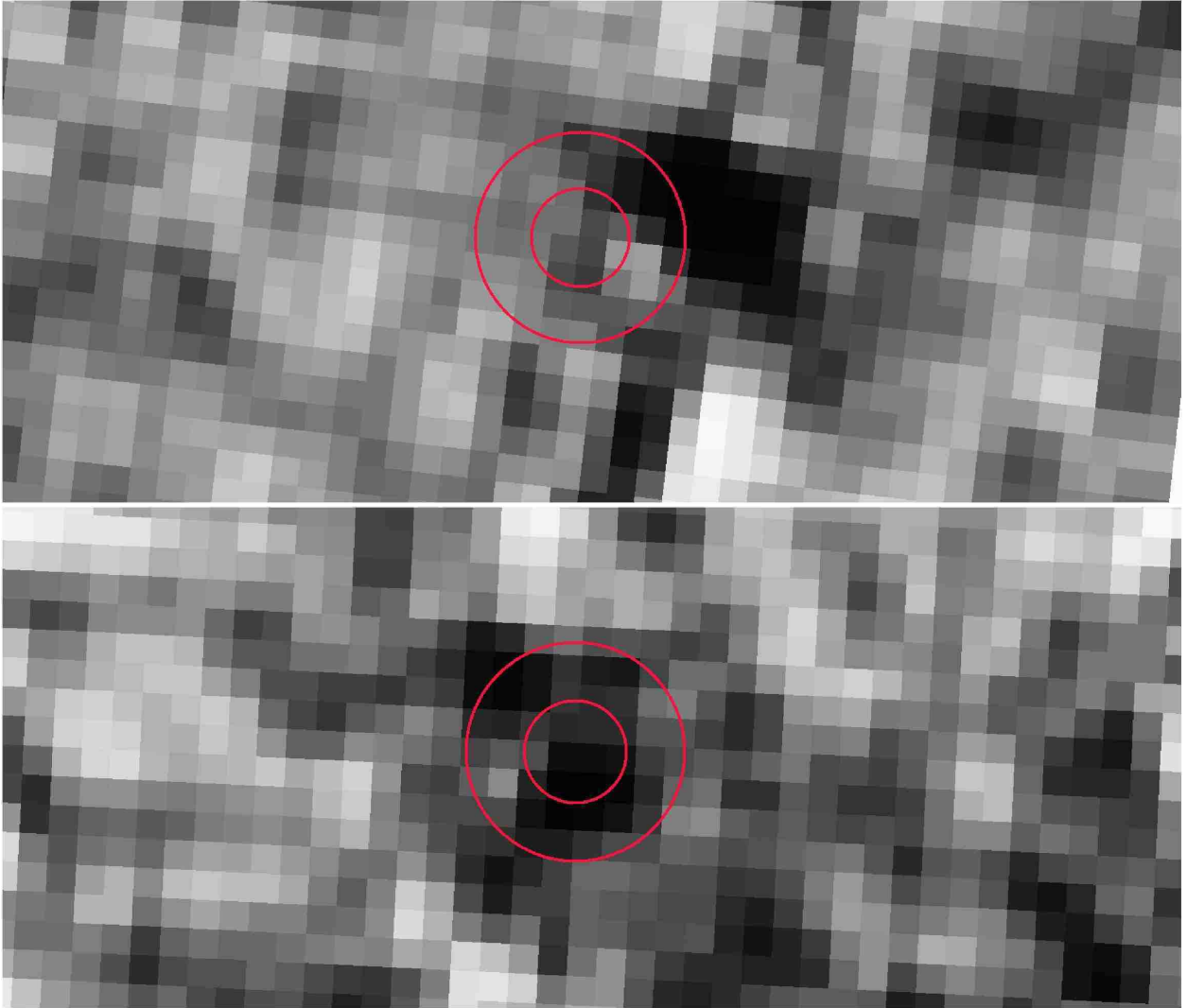


Fig. 4.— The $70\ \mu\text{m}$ *inverted* grayscale mosaics of HD27962 (top) and HD29488 (bottom) resampled to $4''$ pixels in order to gain spatial resolution. North is up and East is to the left in both images. We find that $70\ \mu\text{m}$ emission is detected at a S/N level $\sim 6-7$ within the our aperture (radius= $16''$). However, since the emissions are not centered at the positions of the targets (marked by the concentric circles), we conclude that they are not likely to be associated with them.

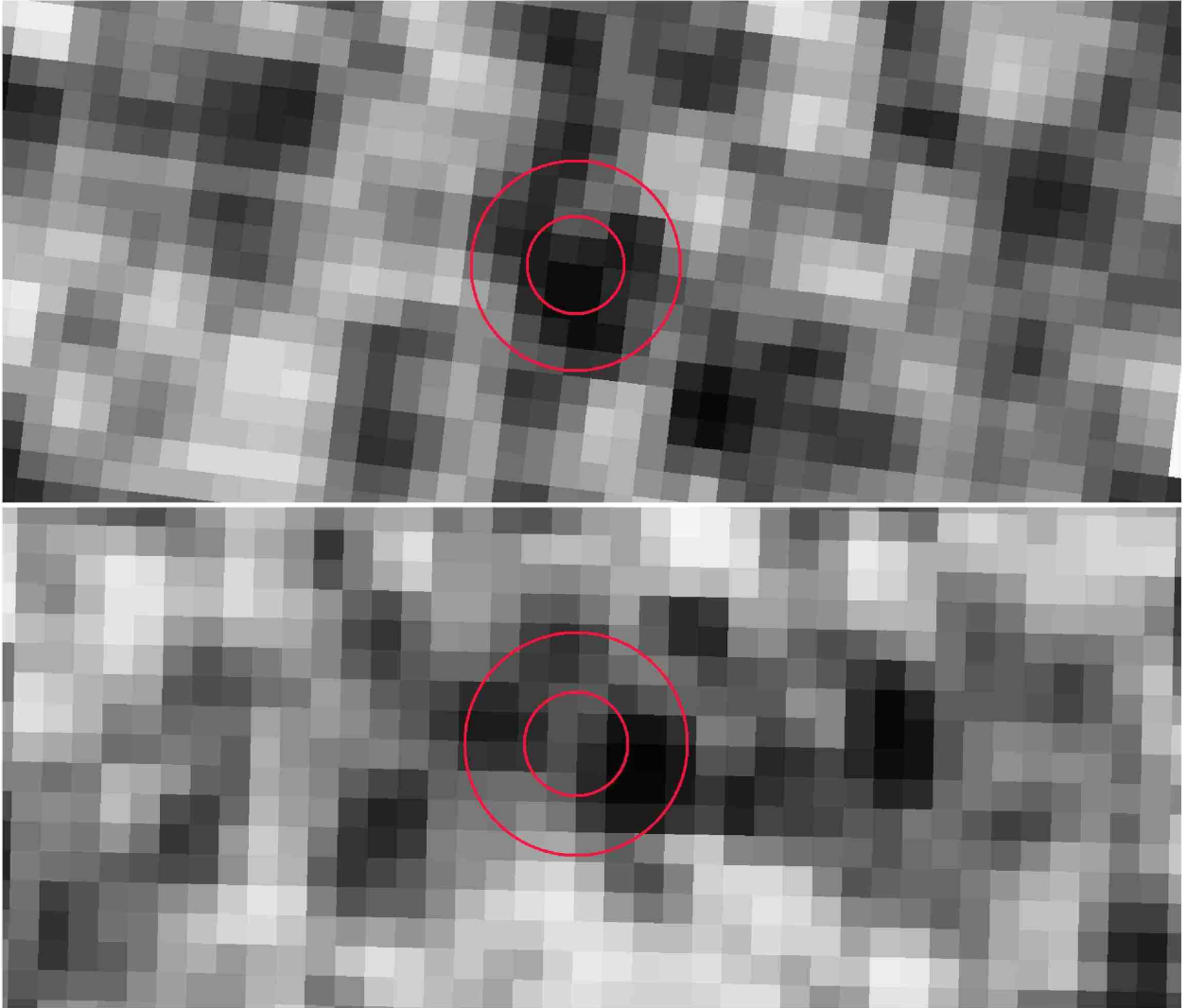


Fig. 5.— The $70\ \mu\text{m}$ *inverted* grayscale mosaics of HD28527 (top) and HD33254 (bottom) resampled to $4''$ pixels in order to gain spatial resolution. North is up and East is to the left in both images. Both objects are A-type stars identified by Su et al. (2006) as having small $70\ \mu\text{m}$ excess ($\text{FLUX}_{70} / L_{*,70} \sim 2.7\text{-}2.9$). However, since we detect these objects at a marginal level ($S/N = 4.9$ and 5.6 , respectively) and the emissions are not centered at the locations of the objects (marked by the concentric circles), we do not consider the detections to be real.

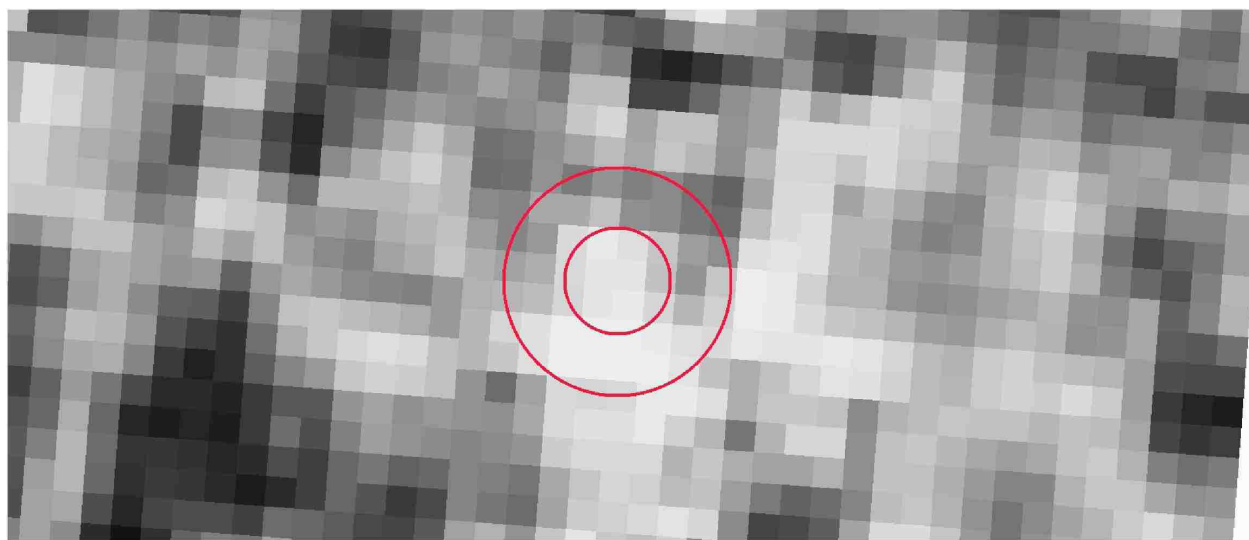


Fig. 6.— The $70\ \mu\text{m}$ *inverted* grayscale mosaic of HD28430 resampled to $4''$ pixels. North is up and East is to the left. Within the aperture centered at the target (marked by the concentric circles), there is a flux deficit that is significant at the $6.9\text{-}\sigma$ level. The existence of this kind of minima strongly suggests that “detections” at the $5\text{-}7\text{-}\sigma$ level should be interpreted with caution.

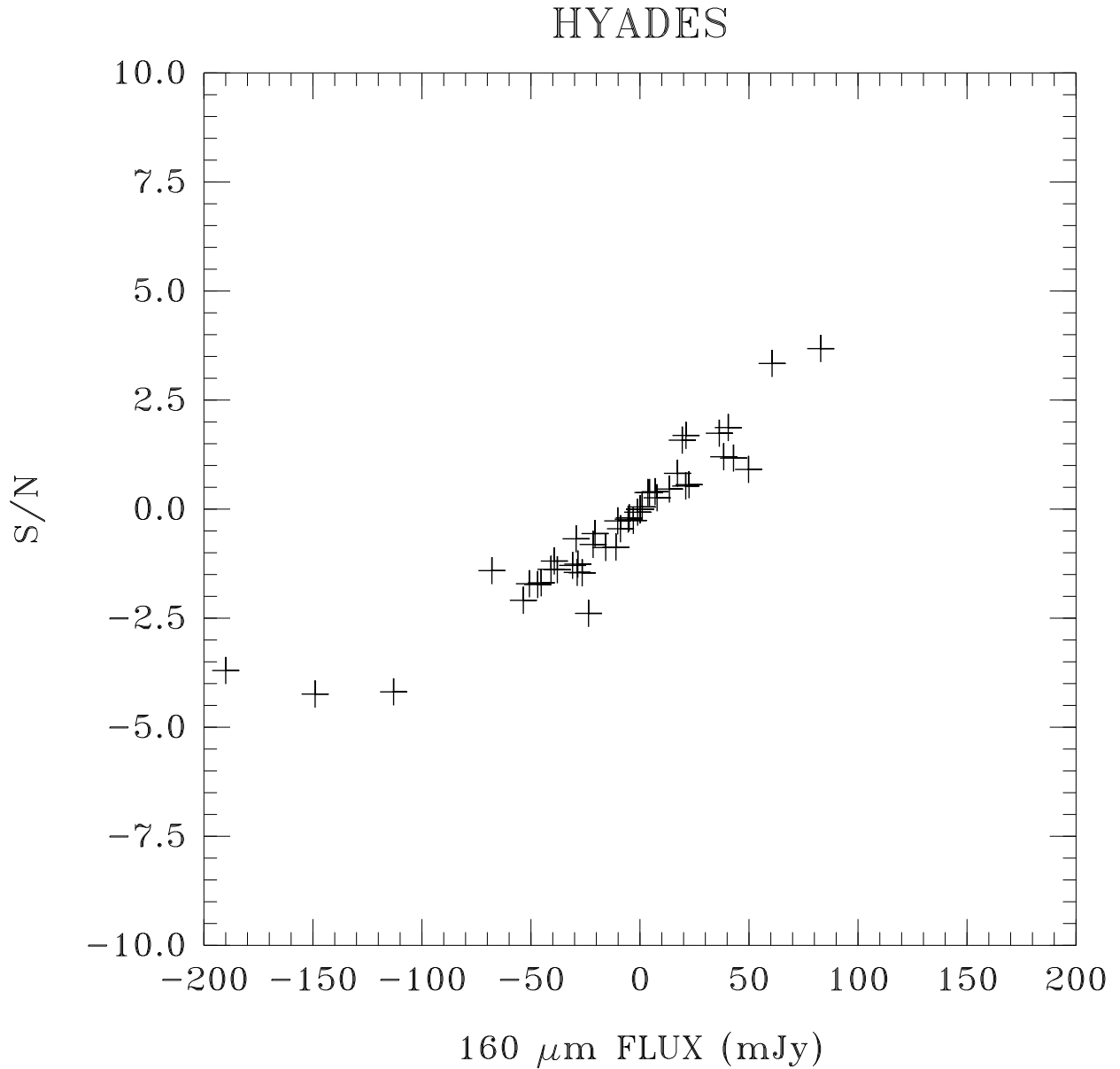


Fig. 7.— The signal to noise ratio versus the measured $160\ \mu\text{m}$ flux for our sample of Hyades stars. We find no obvious $160\ \mu\text{m}$ detections. At $160\ \mu\text{m}$, as at $70\ \mu\text{m}$, the noise is dominated by the extragalactic source confusion and cirrus contamination. Thus, positive and negative fluctuations at the $\sim 5\text{-}\sigma$ level are not uncommon.

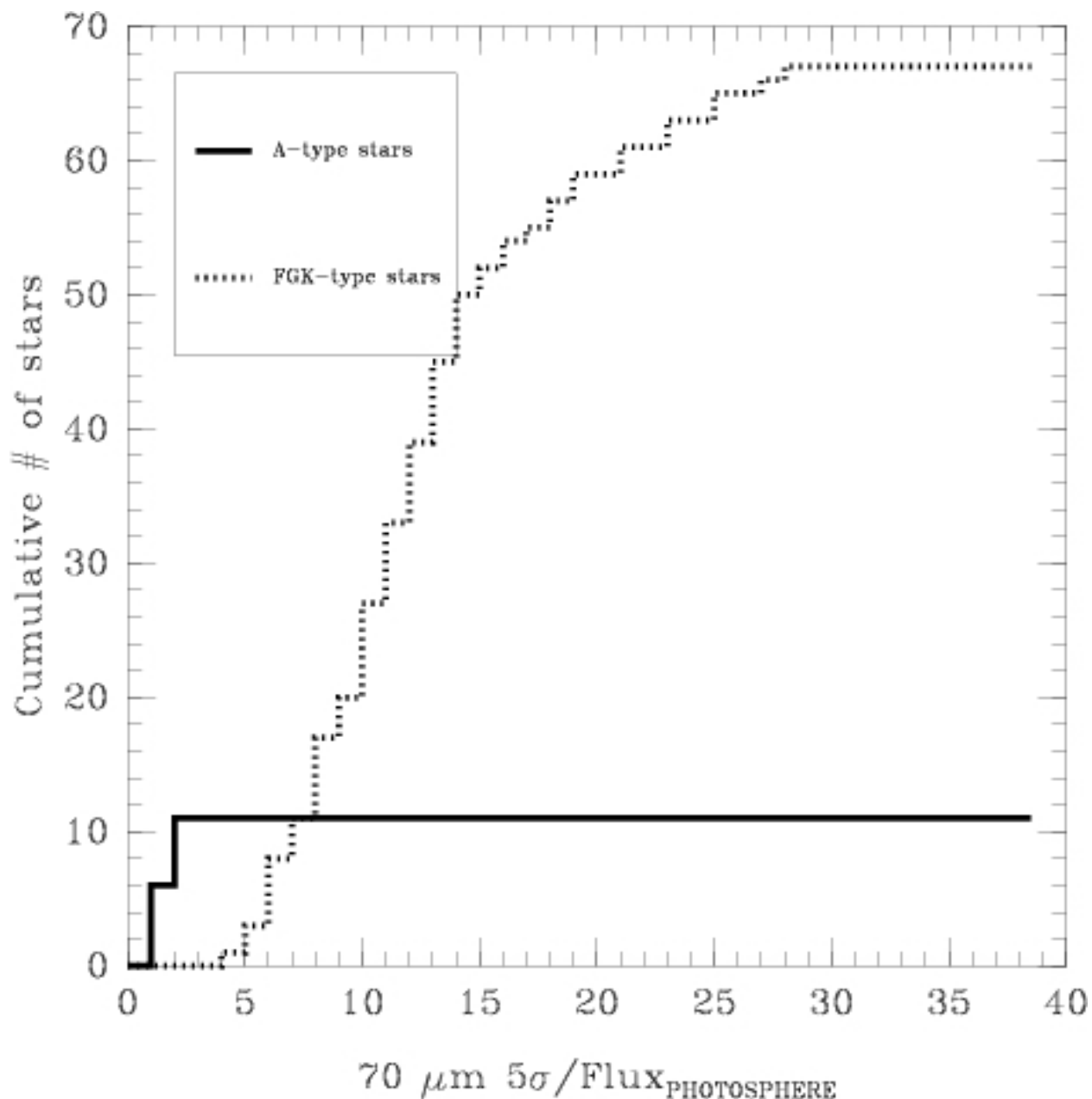


Fig. 8.— Cumulative distribution of $70\ \mu\text{m}$ $5\text{-}\sigma$ sensitivities in units of the expected photospheric fluxes for FGK-type Hyades stars (dotted line) and A-type Hyades stars (solid line). For A-type stars, the $70\ \mu\text{m}$ observations can detect, at the $5\text{-}\sigma$ level, fluxes that are $\sim 1\text{-}2\times$ that of the expected photospheres. In contrast, for most of the FGK-type stars, the $70\ \mu\text{m}$ observations are only sensitive enough to detect fluxes that are $\sim 15\times$ the expected photospheric values.

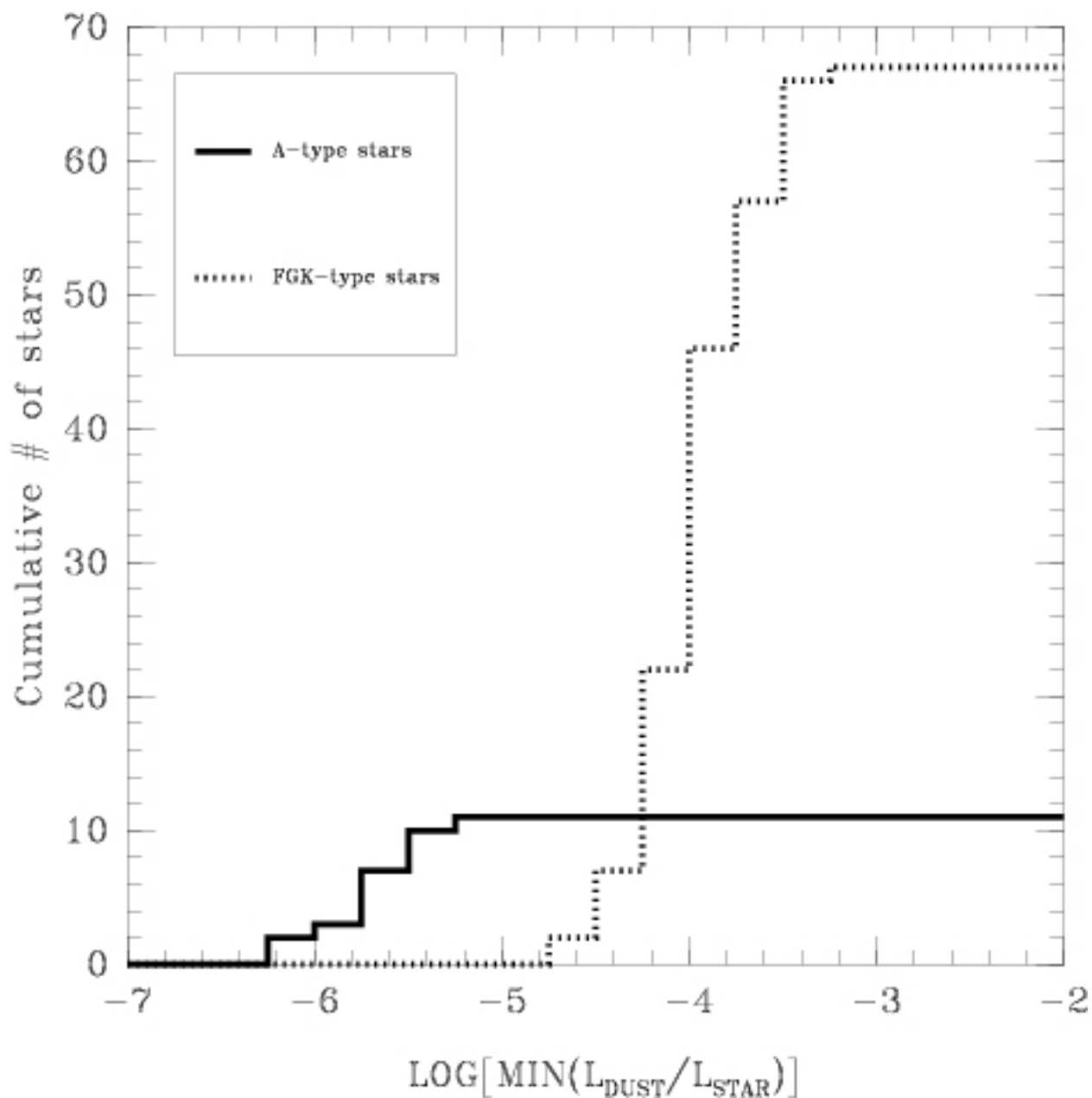


Fig. 9.— Cumulative distribution of $70\ \mu\text{m}$ $5\text{-}\sigma$ sensitivities translated into fractional disk luminosities for FGK-type Hyades stars (dotted line) and A-type Hyades stars (solid line). For A-type stars, the $70\ \mu\text{m}$ observations are sensitive to disks with fractional disk luminosities, L_{DUST}/L_{STAR} , $\sim 5 \times 10^{-6}$. In contrast, for most of the FGK-type stars, the $70\ \mu\text{m}$ observations are only sensitive enough to detect disks with $L_{DUST}/L_{STAR} \gtrsim 2 \times 10^{-4}$.

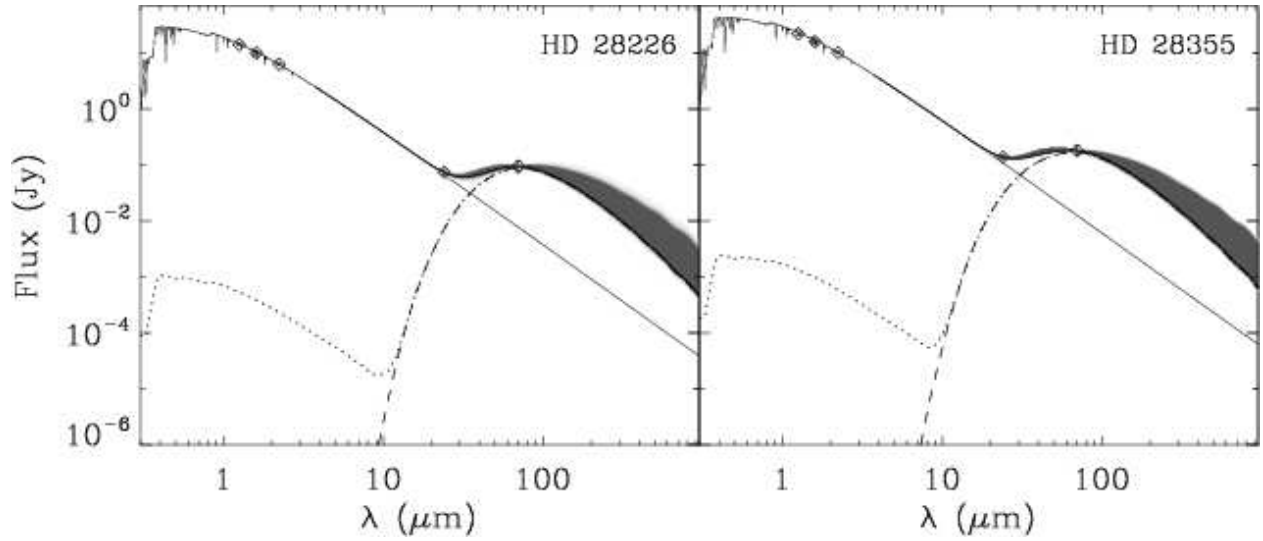


Fig. 10.— Hyades A-type stars with $70 \mu\text{m}$ excess. On each plot, the darkest regions correspond to the most likely fits to the SEDs. The dashed line shows the thermal emission for the best-fit model, while the dotted line corresponds to the total disk emission (i.e. including scattered light emission).

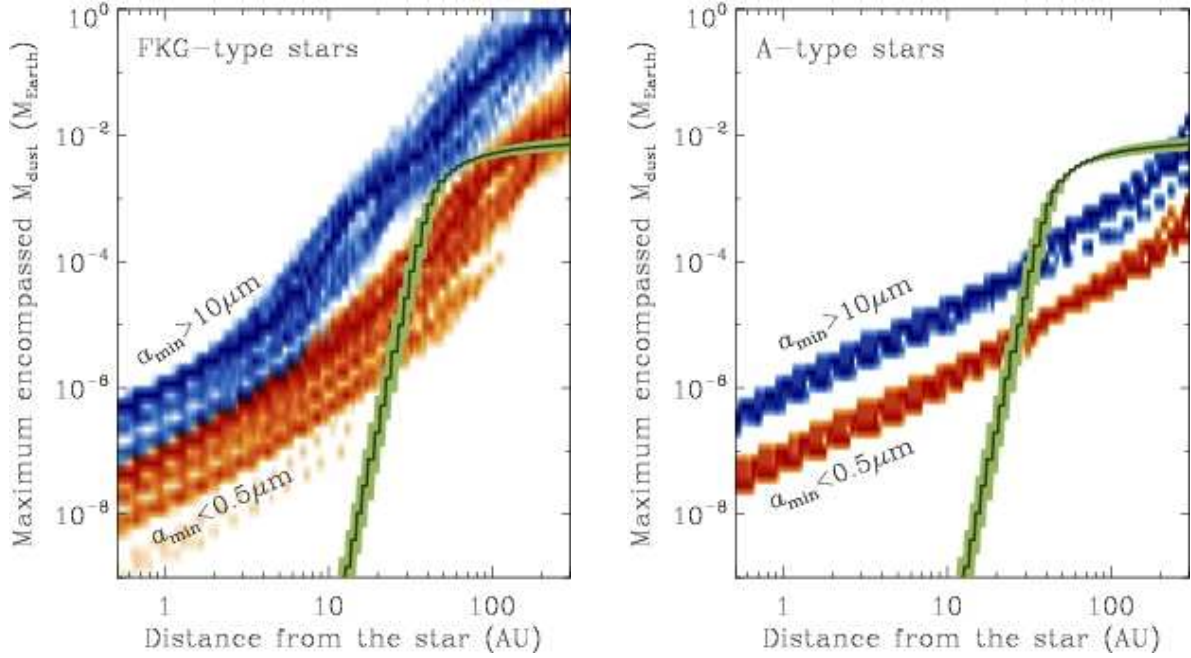


Fig. 11.— Maximum encompassed dust mass as a function of the distance from the star for the FGK and A-type stars without *Spitzer* excesses (respectively left and right panels). The red area corresponds to mass upper limits when minimum grain sizes a_{min} between $0.05 \mu\text{m}$ and $0.5 \mu\text{m}$ are considered, while the blue area corresponds to $10 \mu\text{m} < a_{\text{min}} < 100 \mu\text{m}$. The solid black line corresponds to the mass as a function of radius for the best-fit model of HD 28355 corresponding to the case where $a_{\text{min}} > 10 \mu\text{m}$ (see Table 5). The green region indicates the $1\text{-}\sigma$ limits of the best-fit model.